Thermal and electromechanical response of ultra-thin carbon-strip polarimeter targets in relativistic bunched beams

F. Rathmann, O. Eyser, M. Sangroula, P. Shanmuganathan, V. Shmakova

Brookhaven National Laboratory, Upton, New York

June 2026

Outline

Motivation

- Fast carbon-strip *pC* polarimeters underpin RHIC relative hadron polarimetry.
- EIC demands %-level polarization systematics for protons, use of polarized light ions (d, ^{3}He, ^{6,7}Li) is anticipated.
- In bunched beams the strip is not a passive absorber:
  - bright illumination, deformation, end glow, RF sensitivity, resistance change [1, 2]

Is target survival set by local heating alone, and
will beam scanning using carbon strips still work at the EIC?

Coupled thermal, RF and mechanical model, benchmarked on RHIC.

Carbon-strip target geometry

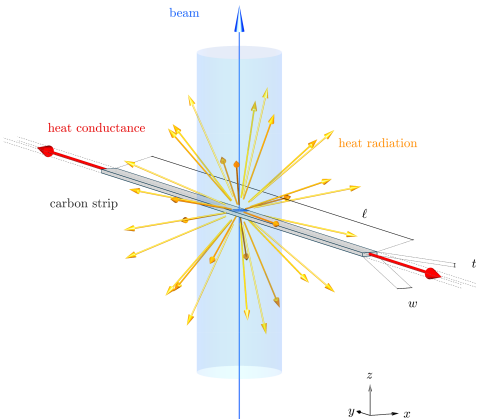

- Strip $\ell \times w \times t$ between two supports.
- Beam along z intercepts the $\ell \times w$ face.
- Cross section $A = wt$: conduction, tension.
- Ideal thermal contact: $T(y = \pm\ell/2) = T_0$.
- Inputs:
  - material: ρ (density), c_p (heat capacity), κ (conductivity), ε (emissivity) ▸ properties
  - state: $R(y)$, σ_{eff} (history dependent)

RHIC reference: $\ell = 25\,\text{mm}$, $w = 10\,\mu\text{m}$, $t = 50\,\text{nm}$, *aspect ratio* $w/t = 200$.

Core damage measure

- A nanometer-scale strip in vacuum has no sharp survival temperature:
  - carbon loss = temperature-dependent rate × exposure time

$$f_{\mathrm{sub}} = \frac{\Delta h_{\mathrm{sub}}}{t}, \qquad \Delta h_{\mathrm{sub}} = \int v_{\mathrm{sub}}\big(T(\tau)\big)\,\mathrm{d}\tau$$

- $v_{\mathrm{sub}}(T)$: surface recession speed from the vapor pressure, exponential in T.
- t: strip thickness; the criterion is the allowed fractional loss over the exposure.

The same $T_{\max}$ can pass a threshold test yet remove the strip: the integral decides.

Observed beam-target response at RHIC

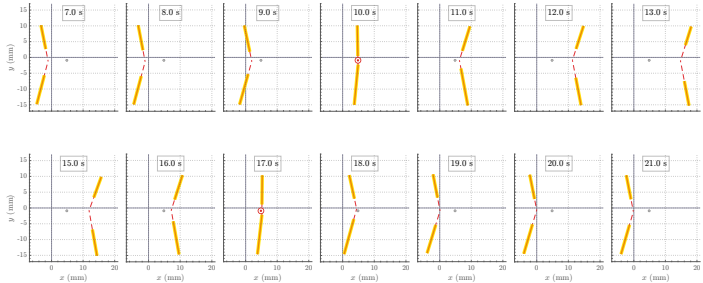

- Deforms toward the beam during scans
- Ends glow *before* interception [1, 2]
- End glow off at lower 200 MHz voltage

▸ end glow

- R: 200–800 MΩ → ∼1 MΩ after beam
- Metal fins near ends improve lifetime

▸ video-derived numbers ▸ force scale

Heating is not confined to the beam spot: the electromagnetic environment matters.

Structure of the response model

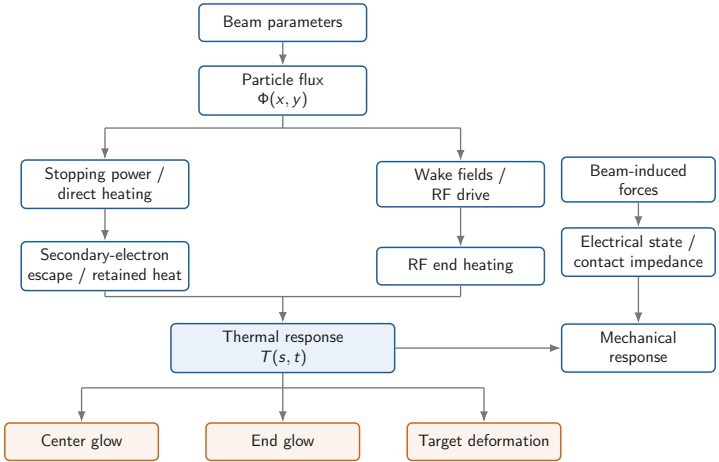

Two heat sources, one electromechanical state.

Beam optics and particle flux

– Gaussian transverse beam, set by the optics at the target location:

$$\sigma_{x,y} = \sqrt{\beta_{x,y}\,\varepsilon_{x,y}} = \sqrt{\frac{\beta_{x,y}\,\varepsilon^{n}_{x,y}}{\beta\gamma}}$$

– Time-averaged particle flux density seen by the target:

$$\Phi(x,y) = \Phi_0 \exp\left[-\frac{x^2}{2\sigma_x^2} - \frac{y^2}{2\sigma_y^2}\right]$$

$$\Phi_0 = \frac{I_{\text{avg}}}{Ze\,2\pi\sigma_x\sigma_y} = \frac{N_b\,N_p\,f_{\text{rev}}}{2\pi\sigma_x\sigma_y}$$

Every heating scale downstream starts from Φ_0: optics and bunch charge define conditions.

Benchmark beam cases

Quantity	Unit	RHIC flattop	EIC inj. before cool.	EIC inj. after cool.	EIC flattop large ε	EIC flattop cooled ε
E_{beam}	GeV	250	23.5	23.5	275	275
N_p	10^{10}	20	27.6	27.6	6.9	6.9
N_b	–	120	290	290	1160	1160
I_{avg}	A	0.30	1.00	1.00	1.00	1.00
$\varepsilon_x^n / \varepsilon_y^n$	µm	2.5 / 2.5	3.3 / 3.3	3.3 / 0.3	3.3 / 3.3	3.3 / 0.3
σ_x	mm	0.49	3.51	3.51	1.61	1.61
σ_y	mm	0.52	2.28	0.69	0.89	0.27
Φ_0	$10^{23}\,\text{m}^{-2}\,\text{s}^{-1}$	11.8	1.24	4.11	6.97	23.1

▸ full parameter table

Cooled vertical emittance doubles Φ_0 over RHIC: → EIC stress case

Particle-flux maps at the target

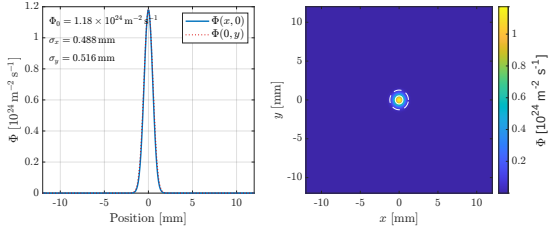

RHIC flattop

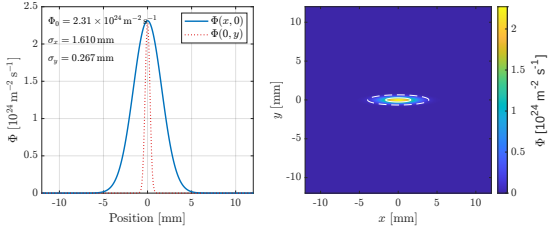

EIC flattop, cooled emittance

– Color: $\Phi(x, y)$; white contours: rms and 95 % beam ellipses. ▸ injection cases

Concentration, not current: Φ_0 spans a factor ∼20 across the benchmark cases.

Beam-target overlap and strip orientation

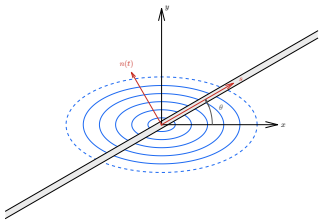

Strip at angle θ to the horizontal beam axis; s along the strip, n normal to it.

centered narrow strip intercepts only $f_{\mathrm{ov}} \simeq w/(\sqrt{2\pi}\,\sigma_\perp)$

- RHIC reference $\ell = 25\,\mathrm{mm}$; $\ell = 50\,\mathrm{mm}$ already fabricated (AGS); longer strips are harder to make

- EIC beams strongly asymmetric: flattop cooled: $\sigma_x^{95} = 3.94\,\mathrm{mm}$, $\sigma_y^{95} = 0.65\,\mathrm{mm}$); optics fixed, the only control is the strip angle θ
- $\sigma_\parallel^2(\theta) = \sigma_x^2 \cos^2\theta + \sigma_y^2 \sin^2\theta$ is the beam projected *along* the strip (it sets the length needed); $\sigma_\perp(\theta)$ the scanned width

$$M_\ell^{95} = \frac{\ell}{2\,\sigma_\parallel^{95}(\theta)}$$

- M_ℓ^{95} = strip ends and holder outside the 95 % envelope, in units of $\sigma_\parallel^{95}$; for a *fixed* ℓ it grows as $\sigma_\parallel^{95}(\theta)$ shrinks ▸ margins
- diagonal $\theta = \pm 45^\circ$ ($\sigma_\parallel = \sigma_\perp = \sqrt{(\sigma_x^2 + \sigma_y^2)/2}$): EIC flattop-cooled M_ℓ^{95} rises 6.3 → 8.9 vs. horizontal, with two symmetric scans that also avoid the worst horizontal width

With ℓ fixed, strip angle is only margin knob, diagonal scans buy most headroom. 10 µm strip intercepts only $\sim 10^{-3}$ to 10^{-2} of beam, but heating is per unit area.

Energy loss in the carbon strip

– tabulated mass stopping power $S_m(E) \rightarrow$ line energy loss in SI units: $S_C^{SI} = 5.123 \times 10^{-11}\,\mathrm{J\,m^{-1}}$ (graphitic/CVD carbon, 250 GeV protons)

$$Q_{\mathrm{loss}}(x,y) = \Phi(x,y)\, S_C^{SI}(E), \qquad Q_{\mathrm{loss},0} = \Phi_0\, S_C^{SI}(E)$$

$$\Delta E_{\mathrm{loss}} = S_C^{SI}(E)\, t \simeq 16.0\ \textbf{eV per proton}\ (t = 50\,\mathrm{nm})$$

– total intercepted power $P_{\mathrm{loss}} = N_b N_p f_{\mathrm{rev}}\, f_{\mathrm{ov}}\, S_C^{SI}(E)\, t$: orientation reduces P_{loss} via f_{ov}, but not the local peak density at beam center

Case	Orientation	f_{ov} $[10^{-3}]$	$Q_{\mathrm{loss},0}$ $[10^{13}\,\mathrm{W\,m^{-3}}]$	P_{loss} $[10^{-2}\,\mathrm{W}]$	$Q_{\mathrm{loss},0}/Q_{\mathrm{loss},0}^{\mathrm{RHIC}}$
RHIC flattop	horizontal	7.724	6.068	3.713	1.000
RHIC flattop	vertical	8.170	6.068	3.928	1.000
EIC injection, no cooling	diagonal	1.346	0.635	2.157	0.105
EIC injection, cooling	diagonal	1.576	2.107	2.525	0.347
EIC flattop, no cooling	diagonal	3.069	3.572	4.920	0.589
EIC flattop, cooling	diagonal	3.456	11.85	5.541	1.953

In a 50 nm strip, energy lost is not energy retained: secondary electrons carry much of it away. ▸ Bethe–Bloch

Secondary-electron escape

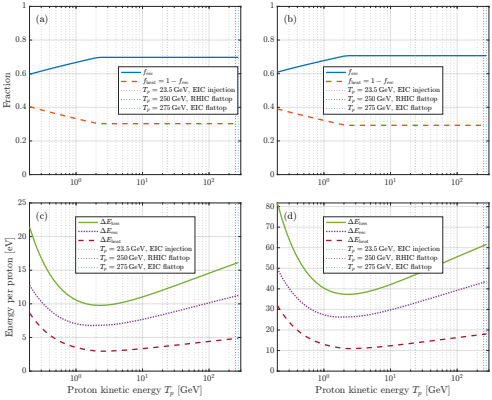

(a,c): ideal flat layer, path length = t; (b,d): roll-averaged rectangular strip (Fig. 4).

$$S_{\rm C}^{\rm SI} = S_{\rm heat} + S_{\rm esc}, \quad f_{\rm esc} = \frac{S_{\rm esc}}{S_{\rm C}^{\rm SI}}$$

- electron escape length $\gtrsim t = 50\,\text{nm}$: thick-target assumption fails
- roll-averaged strip ($w = 10\,\mu\text{m}$): mean proton chord $\langle \ell_{\rm chord} \rangle_\psi = 3.82\,t$ through the curled cross section; energy/proton in (c,d) $= S_{\rm C}^{\rm SI} \times$ path (t or chord) ▸ chord
- plateau above the ionization minimum: the relativistic rise is carried by escaping delta electrons, $\Delta E_{\rm heat}$ stays flat ▸ energy dep.

$f_{\rm esc} \simeq 0.70$ **at RHIC and EIC energies**

About 70 % of the stopping-power loss escapes the 50 nm strip as energetic electrons.

Heat retained in the target

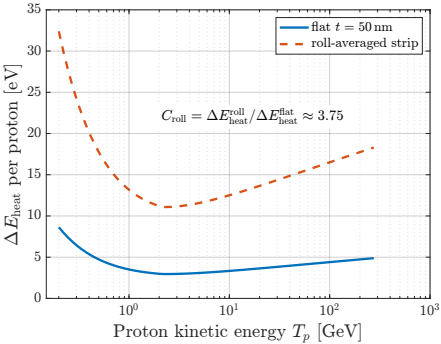

Deposited heat per proton: ideal flat layer vs roll-averaged strip (Fig. 5).

$$C_{\rm roll} = \Delta E^{\rm roll}_{\rm heat}/\Delta E^{\rm flat}_{\rm heat} \approx 3.75$$

$$Q_{\rm heat}(x,y) = \eta_{\rm heat}(E)\, Q_{\rm loss}(x,y)$$

- $f_{\rm heat} = 1 - f_{\rm esc}$: fraction retained within a given geometry; ideal flat layer: $\eta_{\rm heat} = f_{\rm heat} \approx 0.30$
- roll-averaged strip: retained fraction $\times$ chord gain, $\eta_{\rm heat} = \langle f_{\rm heat}\rangle_\psi \, \langle \ell_{\rm chord}\rangle_\psi / t \simeq 0.30 \times 3.82 \approx 1.13$ (RHIC): the longer chord offsets the escape loss; the flat layer is the lower-bound heating case

Case	T_p [GeV]	$\Delta E^{\rm roll}_{\rm heat}$ [eV/proton]	$\eta_{\rm heat}$
EIC injection	22.6	13.9	0.87
RHIC flattop	249.1	18.1	1.13
EIC flattop	274.1	18.3	1.14

Escape and the longer rolled chord nearly cancel: $\eta_{\rm heat} \approx 1$ at RHIC and EIC energies.

Target motion through the beam

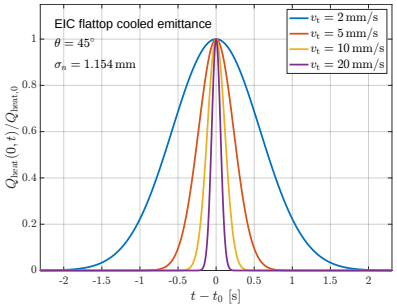

Heat-source pulse at the strip element crossing beam center; EIC flattop cooled, $\theta = 45°$, $\sigma_n = 1.154\,\mathrm{mm}$ (Fig. 7).

- constant-speed scan normal to the strip: $n(t) = n_0 + v_t(t - t_0)$; a material element sees a Gaussian pulse $Q_{\mathrm{heat}}(0,t)/Q_{\mathrm{heat},0} = \exp[-v_t^2(t - t_0)^2/(2\sigma_n^2)]$
- faster motion narrows the pulse, but the peak stays $Q_{\mathrm{heat},0}$

$$\tau_{\mathrm{exp}} \sim \frac{\sigma_n}{v_t}$$

exposure time in the beam core: the operational control parameter for the transient temperature

video-derived $v_t \simeq 4\,\mathrm{mm\,s^{-1}} \rightarrow \tau_{\mathrm{exp}} \simeq 0.3\,\mathrm{s}$

Motion controls the exposure time in the beam core, not the peak heating.

Thermal response: heat-balance equation

- $\ell \gg w, t$: one-dimensional field $T(s,\tau)$ along the strip; cross section enters via $A = wt$ (conduction) and $p_{\mathrm{rad}} = 2(w+t)$ (radiating perimeter)

$$\underbrace{\rho c_p A \frac{\partial T}{\partial \tau}}_{\text{heat storage}} = \underbrace{\frac{\partial}{\partial s}\left(\kappa A \frac{\partial T}{\partial s}\right)}_{\text{axial conduction}} - \underbrace{\varepsilon \sigma_{\mathrm{SB}}\, p_{\mathrm{rad}} \left[T^4(s,\tau) - T_0^4\right]}_{\text{radiative cooling}} + \underbrace{A\, Q_{\mathrm{heat}}(s,\tau)}_{\text{beam source}}$$

- each term is power per unit strip length; dividing by $\rho c_p A$ gives the local heating rate, with thermal diffusivity $\alpha = \kappa/(\rho c_p)$
- boundary and initial conditions: ideal thermal contact to the holder, $T(\pm\ell/2,\tau) = T_0$, $T(s,0) = T_0 = 300\,\mathrm{K}$
- radiation is the only nonlinear term: strong cooling at high T, weak again as the strip cools toward T_0

Formalism and constants: [3, 4]. Material inputs (graphitic/CVD baseline, Table VII): $\kappa = 5\,\mathrm{W\,m^{-1}\,K^{-1}}$, $\rho = 1700\,\mathrm{kg\,m^{-3}}$, $c_p = 750\,\mathrm{J\,kg^{-1}\,K^{-1}}$, $\varepsilon = 0.85$; $w = 10\,\mu\mathrm{m}$, $t = 50\,\mathrm{nm}$, $\ell_{\mathrm{RHIC}} = 25\,\mathrm{mm}$, $\ell_{\mathrm{EIC}} = 50\,\mathrm{mm}$. ▸ input

Heat storage, conduction along strip, and surface radiation balance beam source.

Static steady-state temperature profiles

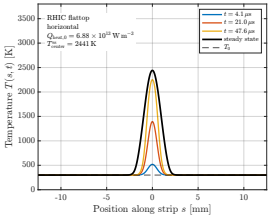

RHIC flattop, horizontal.

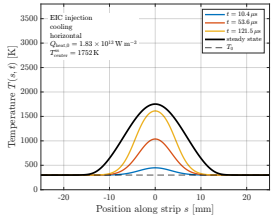

EIC injection, after cooling.

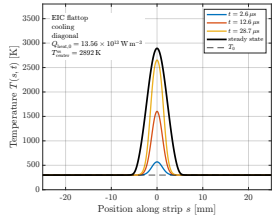

EIC flattop, cooled emittance.

- steady state, $\partial T/\partial \tau = 0$: conduction to the ends and radiation balance the centered source (intermediate times and final profile)
- continuous exposure of the same strip element: conservative upper-limit benchmark, not normal operation
- peak temperature set by the local $Q_{\mathrm{heat},0}$, essentially independent of orientation; inclination changes only the profile width via $\sigma_{\parallel}(\theta)$

$T^{\mathrm{ss}}_{\mathrm{center}} \simeq 2441\,\mathrm{K}$ **(RHIC)** $1752\,\mathrm{K}$ **(EIC injection)** $2892\,\mathrm{K}$ **(EIC flattop cooled)**

EIC flattop cooled is the static worst case: 2892 K; survival is a sublimation-rate question, not a threshold.

Temperature with moving target

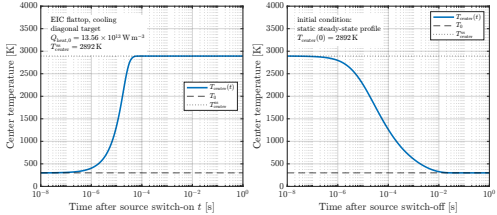

Center temperature after source switch-on from T_0 (left) and after switch-off from the steady state (right).

- $\tau_{\mathrm{exp}} \gg$ thermal rise time: scan thermally quasi-static, $T^{\mathrm{peak}}_{\mathrm{max}} = 2892\,\mathrm{K}$ (static benchmark)
- motion alone: reducing EIC peak to RHIC proton static level requires $v_{\mathrm{t}} \simeq 82\,\mathrm{m\,s^{-1}}$ ($\tau_{\mathrm{exp}} \simeq 1.4 \times 10^{-5}\,\mathrm{s}$)
- inertia: $a \simeq 4v^2_{\mathrm{avg}}/s_{\mathrm{travel}} \approx 9 \times 10^5\,\mathrm{m\,s^{-2}}$ over $\sim$30 mm: $\rightarrow$ breaking scale $\frac{\sigma_{\mathrm{break}}}{(\rho\ell)} \sim 10^6\,\mathrm{m\,s^{-2}}$
- higher speed: detected events per pass scale with $\tau_{\mathrm{exp}} \propto 1/v_{\mathrm{t}}$, factor $\sim 2 \times 10^4$ fewer at $82\,\mathrm{m\,s^{-1}}$
- optics alternative: $Q_{\mathrm{heat},0} \propto 1/(\sigma_x\sigma_y)$: a factor $\simeq 1.97$ larger beam area ($\beta_x, \beta_y \rightarrow 2\beta$) reaches the RHIC proton source level
- cooling is $\sim$100$\times$ slower than heating: radiation $\propto T^4$ fades as the strip cools

At 4 mm s^{-1}, scan is thermally quasi-static: the strip reaches the full static temperature.

Power scale of the observed end glow

- strip ends glow *before* direct beam interception; the glow ceases when the 200 MHz cavity voltage is lowered: a nonlocal, RF-driven heat source ▸ observations
- video inputs: glowing length $\ell_{\mathrm{end}} \simeq 8\,\mathrm{mm}$; apparent yellow color, compared with an oven glow, suggests $T_{\mathrm{end}} \simeq 1200\,^{\circ}\mathrm{C} \simeq 1470\,\mathrm{K}$ (not calibrated pyrometry)

$$P_{\mathrm{rad,end}} \simeq \varepsilon\,\sigma_{\mathrm{SB}}\,p_{\mathrm{rad}}\,\ell_{\mathrm{end}}\left(T_{\mathrm{end}}^{4} - T_{0}^{4}\right) \simeq 36\,\mathrm{mW}$$

- per glowing end region; dominant uncertainties are emitting length, emissivity, and optical temperature
- unexposed micro-ribbons: $R \simeq 200$ to $800\,\mathrm{M\Omega}$ over 25 mm, so $R_{\mathrm{end}} \simeq 64$ to $256\,\mathrm{M\Omega}$ for 8 mm end segment

$$I_{\mathrm{RF,rms}} = \sqrt{P_{\mathrm{end}}/R_{\mathrm{end}}} \simeq 12 \textbf{ to } 24\,\boldsymbol{\mu}\mathbf{A} \quad \rightarrow \quad V_{\mathrm{RF,rms}} \simeq 1.5 \textbf{ to } 6\,\mathbf{kV}$$

End-glow and resistance observations: [1, 2]. These scales are the benchmark for wakefield estimates on the next slide.

Tens of μA through high-resistance strip ends suffice: the required drive is kV-scale, not watts.

Effective RF-current model for strip-end heating

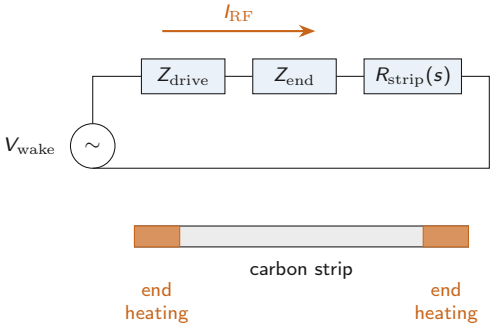

$$Q_{\mathrm{tot}}(s,t) = Q_{\mathrm{heat}}(s,t) + Q_{\mathrm{RF}}(s,t)$$

- end-localized Joule term: $Q_{\mathrm{RF}} = p'_{\mathrm{RF}}/A$ with $p'_{\mathrm{RF}}(s,t) = I^2_{\mathrm{RF}}(t)\,R'(s,t)$, primes denoting power and resistance per unit strip length: dissipation concentrates where R' is largest
- resistance is a history-dependent state variable $R_{\mathrm{strip}} \to R(s,t)$: the beam-exposed center graphitizes to $\sim$1 MΩ, the ends stay at hundreds of MΩ [1, 2]
- hence the ends glow before the low-resistance center ever intercepts the beam
- Q_{RF} is not a free fit parameter: normalization from the wakefield drive, spatial shape from holder and contacts, response anchored by the observed glow

RF current through nonuniform resistance heats the ends first, as the videos show.

Wakefields: aluminum vs alumina target holder for the EIC

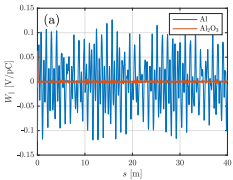

Longitudinal wake potential $W_\parallel(s)$.

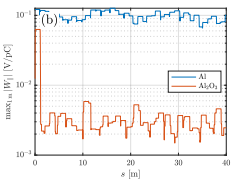

Running max of $|W_\parallel|$, 1 m window.

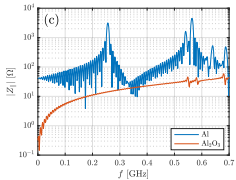

Low-frequency impedance $|Z_\parallel(f)|$.

- peak wake: 0.13 (Al) vs 0.063 V/pC (Al_2O_3), only a factor ∼2; the long-range RMS envelope drops 0.052 → 0.003 V/pC, more than an order of magnitude
- single-bunch voltage scale $|V_{\rm wake}| = |W_\parallel|\, q_b$: for $q_b \simeq 10$ to 20 nC, $|V^{\rm Al}_{\rm wake}| \simeq 1.3$ to 2.6 kV, meeting the kV benchmark of the end-glow estimate
- the 50 nm strip itself cannot be meshed in a cm-scale chamber: it enters later as an effective electrical load

CST wakefield calculation; $\sigma_L = 60$ mm, $N_b = 290$ bunches, $q_b = 30.5$ nC.

Holder wakefields supply the kV-scale drive; Al_2O_3 kills the persistent envelope, not the local peak.

Holder geometry and surface conductivity for the EIC

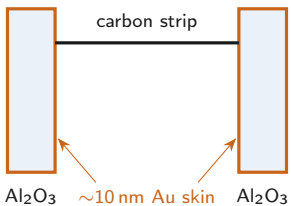

end response involves only
$\sim 10^5$ **to** 10^6 **electrons**
so available charge supply matters

- the relevant design quantity is the electromagnetic boundary condition at the strip ends, not "insulating vs conducting" per se
- solid metal holder: well-defined boundaries, but strong coupling, large wake amplitudes, persistent envelope, and impedance peaks near the ends
- Al_2O_3 body: suppresses the persistent wake envelope and the low-frequency impedance structure; the largest local excursion remains
- thin Au skin: keeps the ceramic from charging up, yet stores far less charge than solid metal, throttling the transient charge buildup that feeds end heating
- consistent with RHIC: rounded metal fins improved lifetime, but the end environment still had to be controlled

A dielectric body with a thin conducting skin starves the end region of charge.

Force scale for visible strip displacement

- observed symmetry: the strip is deflected *toward* the beam from either side, and the sign reverses after the target crosses the beam: not a fixed-direction push ▸ observations
- the deformation is visible over many millimeters, which constrains short-ranged force mechanisms
- slack-string model: two straight segments joined at the displacement maximum, restoring force from the axial tension $T = \sigma_{\mathrm{eff}} A$

$$F_{\mathrm{mech}} \simeq 2T \sin\theta \simeq \frac{4T}{L}\,\Delta x \;=\; 2.4 \times 10^{-7}\,\mathrm{N}\left(\frac{\sigma_{\mathrm{eff}}}{1\,\mathrm{MPa}}\right)$$

- video inputs: $L = 25\,\mathrm{mm}$, $\Delta x_{\mathrm{proj}} \simeq 3\,\mathrm{mm}$; σ_{eff} is the mounted-strip stress, a model parameter distinct from the residual film stress ($\sigma_{\mathrm{eff}} \sim 0.1$ to $10\,\mathrm{MPa}$)
- beam-hit frames show a straight projection: the slack must lie out of the camera plane, along $\pm z$, where the Lorentz force on a radial strip current points

$$F_{\mathrm{mech}} \sim 10^{-8} \text{ to } 10^{-6}\,\mathrm{N}, \quad \text{strip weight only } mg \simeq 2 \times 10^{-10}\,\mathrm{N}$$

Visible deflection needs 10^{-8} to 10^{-6} N, up to 10^{4} times the strip's own weight.

Which force mechanism fits the observations?

- **magnetic Lorentz force:** the beam field is azimuthal, so a radial strip current gives a force along $\pm z$, not the observed radial attraction; it instead explains why the slack hides out of the camera plane
- **net or local charge:** beam field $E(5\,\mathrm{mm}) \simeq 8.4 \times 10^4\,\mathrm{V\,m^{-1}}$; a force of $10^{-8}\,\mathrm{N}$ requires only $q \simeq 1.2 \times 10^{-13}\,\mathrm{C} \simeq 7 \times 10^5$ electrons: a very small imbalance for a connected strip-holder system, with the right attractive symmetry from either side
- **polarization of an isolated strip:** correct symmetry, but $F_{\mathrm{pol}} \propto 1/r^3$: even the flat-ribbon estimate falls from $6 \times 10^{-9}\,\mathrm{N}$ at 1 mm to $5 \times 10^{-11}\,\mathrm{N}$ at 5 mm, too short-ranged for the mm-scale deformation pattern
- **bunch-driven charge redistribution:** relaxation $\tau_{RC} = R_{\mathrm{eff}} C_{\mathrm{eff}} \sim 0.1\,\mu\mathrm{s}$ to $300\,\mu\mathrm{s}$ far exceeds the 107 ns RHIC bunch spacing where the deformation was observed (EIC: 11 to 44 ns, shorter still), so charge need not return to equilibrium between bunches; the same oscillating $\tilde{q}(t)$ drives the RF current ($I_{\mathrm{RF}}^{\mathrm{rms}} \sim 10$ to $25\,\mu\mathrm{A}$, capacitive voltage $\sim$20 to 400 V)

Charge redistribution explains both attraction and end glow; polarization is too short-ranged.

Force-scale comparison

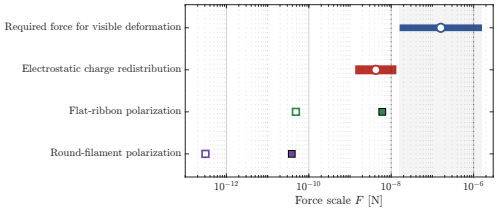

Required force for visible deformation, electrostatic charge-redistribution range (10^5 to 10^6 electrons at $r = 5\,\mathrm{mm}$), and isolated-polarization estimates (filled: $r = 1\,\mathrm{mm}$, open: $r = 5\,\mathrm{mm}$).

- the charge-redistribution range overlaps the required force band; the polarization estimates fall one to four orders of magnitude short and decay as $1/r^3$
- attraction and end glow are distinct local effects of the same electrical response: beam-induced charging, charge redistribution, RF current, and a history-dependent resistance profile
- the resulting picture is coupled electrical, mechanical, and thermal: deformation, pre-interception end glow, RF sensitivity, and resistance history all fit

One electrical response, two symptoms: deformation and end glow.

Carbon sublimation in vacuum: kinetics, not a threshold

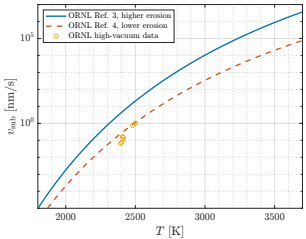

Recession speed from two ORNL vapor-pressure parameterizations; circles: ORNL high-vacuum mass-loss data [5].

$$P_{\rm vap}(T) = P_0 \, \exp\!\left(-\frac{\Delta h_{\rm sub}}{R\,T}\right)$$

the exponential in T behind the steep $v_{\rm sub}(T)$

- no sharp sublimation temperature exists for a nm-scale strip in vacuum: mass loss is set by vapor pressure at the hot surface and the exposure time

$$\Gamma_m(T) \simeq \alpha P_{\rm vap}(T)\sqrt{\frac{M}{2\pi R T}}, \quad v_{\rm sub} = \frac{\Gamma_m}{\rho}$$

- Hertz-Knudsen evaporation flux [6]; vapor-pressure input from graphite data [7, 8]
- damage measure for a strip of thickness t: $f_{\rm sub} = \Delta h_{\rm sub}/t$ with $\Delta h_{\rm sub} = \int v_{\rm sub}(T(\tau))\,\mathrm{d}\tau$
- ORNL data fall on the lower-erosion curve, used for all estimates; the higher curve [9] overpredicts by more than 10×

The relevant limit is the integrated fractional thickness loss, not a sublimation temperature.

From temperature to lifetime: loss timescales

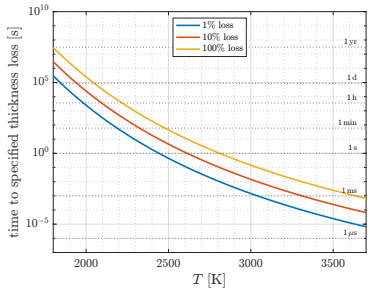

Time to remove 1 %, 10 %, 100 % of a 50 nm strip.

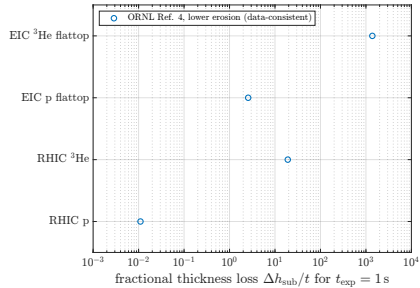

Frac. thickness loss after 1 s at calc. peak temperatures.

- left: temperature axis becomes an allowed dwell time for a given loss budget; steepness reflects exponential vapor pressure
- right: a severity scale, the 1 s normalization does not imply the moving target stays at $T_{\max}$ for 1 s
- RHIC p: $(f_{\mathrm{sub}})_{1\,\mathrm{s}} \simeq 0.011$, about 1 % per second; EIC p flattop: $\simeq 2.6$ strip thicknesses per second; EIC ^{3}He flattop: $\sim 10^3$

At EIC flattop temperatures a 50 nm strip loses its full thickness in well under a second.

Booster and AGS: no thermal concern in the injector chain

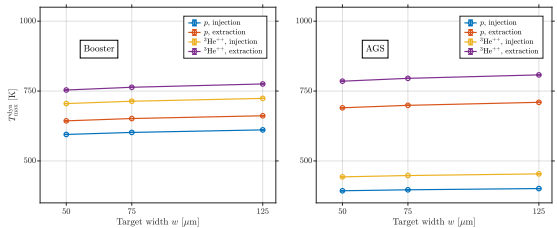

Moving-transient peak temperature vs strip width for proton and $^3\mathrm{He}^{++}$ beams at injection and extraction; $w = 50$, 75, 125 µm, $t = 30$ nm, $\ell = 50$ mm.

- same model and graphitic/CVD baseline; Bethe-Bloch stopping from charge, mass, and velocity: $^3\mathrm{He}^{++}$ carries $z^2 = 4\times$ the proton loss per ion
- all cases stay below ∼810 K; the worst is AGS ^{3}He extraction at 808 K (largest width)
- the width dependence promised earlier: visible but moderate, a few hundred kelvin over $w = 50$ to 125 µm; width is not the dominant control parameter
- vacuum sublimation negligible: $\Delta h_{\mathrm{sub}}/t < 2 \times 10^{-5}$ for 1 s even in the worst case

The injector chain poses no thermal concerns: AGS ^{3}He extraction peaks near 800 K, sublimation negligible.

Machine comparison: peak temperatures and risk

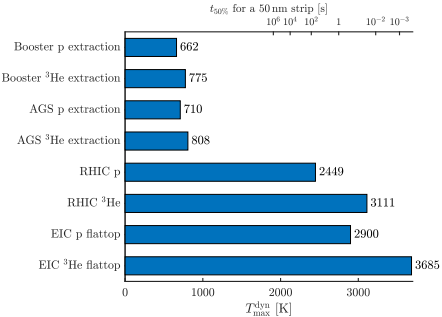

Dynamic peak temperatures for selected cases; upper axis converts temperature to time to remove 50 % of 50 nm strip.

- collider benchmarks (hottest geometry per case): RHIC p 2449 K, RHIC ^{3}He 3111 K, EIC p flattop cooled 2900 K, EIC ^{3}He flattop cooled 3685 K ▸ Table XI
- $t_{50\%}$ axis makes risk ordering immediate: hours at RHIC p shrink to far below 1 s for EIC ^{3}He stress case
- RHIC p is the empirical anchor: a calculated comparison to a regime known to operate, not a measured temperature; static and dynamic values agree (quasi-static scans)

EIC ^{3}He flattop runs 1200 K hotter than the proven RHIC proton point.

RHIC protons: target-lifetime scale from beam-center sublimation

Sublimation loss per measurement cycle

- $\left(f_{\mathrm{sub}}\right)_{1\,\mathrm{s}} \simeq 0.011$ at $T_{\mathrm{max}}^{\mathrm{dyn}} \simeq 2449\,\mathrm{K}$ (RHIC proton source level), lower-erosion recession curve [5, 8]
- Video-derived $\Delta t_{\mathrm{beam}} \simeq 1.5\,\mathrm{s}$ per pass; in-and-out cycle $\Delta t_{\mathrm{cycle}} = 2\,\Delta t_{\mathrm{beam}} \simeq 3\,\mathrm{s}$

$$\left(f_{\mathrm{sub}}\right)_{\mathrm{cycle}} \simeq \Delta t_{\mathrm{cycle}} \left(f_{\mathrm{sub}}\right)_{1\,\mathrm{s}} \simeq 0.033$$

$\sim$3 % of the 50 nm strip per in-and-out cycle

Cycles to 50 % loss, $N_{\mathrm{cycle}} = 0.5/(f_{\mathrm{sub}})_{\mathrm{cycle}}$

- Peak intensity: $N_{\mathrm{cycle}} \simeq 15$ (lower bound)
- Cycle-averaged $\langle I \rangle \simeq 0.8\, I_{\mathrm{peak}}$: $T \propto I^{1/4} \Rightarrow 2316\,\mathrm{K}$, f_{sub} down $\sim$8-fold: $N_{\mathrm{cycle}} \simeq 120$ (upper bound)

Observed lifetimes [2]

- 2013, no fins: avg. 27 $\rightarrow$ near lower bound
- 2015, fins: avg. 142 (best 396) $\rightarrow$ at and above upper bound

Beam-center heating reproduces the lifetime scale; the fin gain validates the end-heating mechanism.

EIC extrapolation: the same cycle estimate at flattop temperatures

The conservative RHIC-like cycle, $\Delta t_{\mathrm{cycle}} \simeq 3\,\mathrm{s}$, applied to the EIC cooled-emittance flattop cases:

EIC p flattop, cooled emittance

- $T_{\mathrm{max}}^{\mathrm{dyn}} \simeq 2900\,\mathrm{K}$ gives $\left(f_{\mathrm{sub}}\right)_{1\,\mathrm{s}} \simeq 2.6$, already on the data-driven lower-erosion curve

$$\left(f_{\mathrm{sub}}\right)_{\mathrm{cycle}} \simeq 7.7$$

- More than one full strip thickness lost per cycle: not a straightforward extrapolation of RHIC proton operation at same dwell time

EIC ^{3}He flattop, cooled emittance

- $T_{\mathrm{max}}^{\mathrm{dyn}} \simeq 3685\,\mathrm{K}$ drives the one-second loss far higher

$$\left(f_{\mathrm{sub}}\right)_{1\,\mathrm{s}} \gtrsim 10^3$$

- Beyond carbon-strip operation with RHIC-like scan times: requires much shorter dwell near the beam core, a smaller peak heat source, or a different target concept or technology

EIC flattop loss exceeds the strip itself: p one full thickness per cycle, ^{3}He far more.

Target-geometry dead ends

Thinner strips do not run cooler

- Deposited energy, thermal mass, and conductive cross section all scale with the thickness t: thinning does not lower the peak temperature in proportion
- A fixed recession depth Δh_{sub} is a larger fractional loss $f_{\mathrm{sub}} = \Delta h_{\mathrm{sub}}/t$ for a thinner strip
- Width, scan speed, and dwell time are the relevant operational controls, not thickness reduction alone

Thicker targets remove the beam

Survival-equivalent scale-up $F_A = A_{\mathrm{C}}/A_{\mathrm{C},0}$: carbon cross section needed to restore RHIC-like measurement numbers (order-of-magnitude factors, not design values)

Case	F_A	$\Delta_{\mathcal{L}}$ per fill
RHIC p, nominal strip	1	$(6.3\text{–}7.5) \times 10^{-5}$
EIC p flattop	2.1×10^2	1.3–1.6 %
RHIC ^{3}He	2.0×10^3	38.5 %
EIC ^{3}He flattop	1.7×10^5	$\simeq 100$ %

$\Delta_{\mathcal{L}}$: luminosity-weighted beam loss per fill, three in-and-out measurements per fill

▸ full table ▸ Thieberger comparison

Thickness is no control knob: thinner strips lose faster, thicker targets consume the beam.

Mitigation paths for carbon-strip survival

1. **Reduce target dwell time:** $f_{\mathrm{sub}} \propto 1/v_t$ for target speed v_t. Going from the observed $v_t \simeq 4\,\mathrm{mm/s}$ to $\simeq 4\,\mathrm{m/s}$ cuts the dwell-time loss by $\sim 10^3$, bringing EIC p flattop near the RHIC p scale.
   - The required acceleration, $\simeq 2.1 \times 10^3\,\mathrm{m/s^2}$, is far below the $\sim 10^6\,\mathrm{m/s^2}$ inertial breaking scale: actuator dynamics, vibration, slack-strip modes, and contacts limit first, not strip inertia.
   - The shorter dwell costs the same factor $\sim 10^3$ in events collected per pass.
2. **Match detector acceptance to faster scans:** a smaller target–detector distance r raises the solid angle as $1/r^2$, so a threefold smaller distance gains roughly a factor 10; with larger detector area, improved readout, or a modified scan strategy on top, the recovery still falls well short of the $\sim 10^3$ events lost to the faster scan
3. **Change beam optics:** larger beam size, lower peak flux, or reduced bunch intensity lower the thermal source, but these are machine parameters, not polarimeter-only knobs
4. **Suppress RF-induced end heating:** low-conductivity holders (alumina) improve the electromagnetic environment at the strip ends [2]; this addresses end losses, not beam-center sublimation
5. **Develop new target or diagnostic technology:** EIC ^{3}He flattop loses $\sim 10^3$ strip thicknesses per second, heavier species (^{6,7}Li) more: renewable, pellet-style, or tape targets, alternative low-Z materials, or non-invasive spin diagnostics [10]

No single fix helps alone: EIC p an interim fix at best, ^{3}He needs a new technology.

Conclusions

Two opening questions: is survival local heating alone (1), and does carbon-strip scanning reach the EIC (2)?

1. The RHIC experience is a coupled target-response problem

- Not local stopping-power heating alone: end glow requires an RF heating channel, the deformation a transverse electrostatic force
- The thermal calculation reproduces the RHIC proton lifetime scale (15–120 cycles vs. observed 27–142); the fin gain confirms the end-heating channel

2. Scanning carbon strips do not extrapolate to the demanding EIC light-ion cases

- EIC p flattop loses $\left(f_{\mathrm{sub}}\right)_{\mathrm{cycle}} \simeq 7.7$ strip thicknesses per RHIC-like in-and-out cycle: dwell, acceptance, and end-heating measures are an interim fix only
- EIC ^{3}He cooled emittance loses $\simeq 2 \times 10^3$ thicknesses per single 1.5 s pass: beyond practical operation; with $\mathrm{d}E/\mathrm{d}x \propto z_{\mathrm{ion}}^2$, $^{6,7}\mathrm{Li}^{3+}$ is another factor $9/4 \simeq 2.25$ above $^3\mathrm{He}^{++}$
- Outlook: develop a different technique in parallel. Tracked pellet targets (laser plus line-scan-camera tracking) could preserve the profile information now obtained by scanning [11, 12]

A different polarimetry technique must be developed in parallel for the EIC light-ion program.

References

[1] D. B. Steski, L. Sukhanova, A. Zelenski, and W. B. Christie. Recent developments in the production of carbon micro-ribbons for CNI polarimeters at BNL. *Journal of Radioanalytical and Nuclear Chemistry*, 299:1035–1039, 2014. doi:10.1007/s10967-013-2646-0.

[2] D. B. Steski, H. Huang, J. Kewisch, L. Sukhanova, and A. Zelenski. Improvements of the target lifetime in the RHIC polarimeter. In *Proceedings of the 28th World Conference of the International Nuclear Target Development Society*, volume 1962 of *AIP Conference Proceedings*, page 030017. AIP Publishing, 2018. doi:10.1063/1.5035534.

[3] Richard Becker. *Theory of Heat*. Springer-Verlag, 1985.

[4] David W. Hahn and M. Necati Özisik. *Heat Conduction*. Wiley, 3 edition, 2012. doi:10.1002/9781118411285.

[5] J. R. Haines and C. C. Tsai. Graphite sublimation tests for the Muon Collider/Neutrino Factory target development program. Technical Report ORNL/TM-2002/27, Oak Ridge National Laboratory, Oak Ridge, TN, USA, February 2002. U.S. DOE contract DE-AC05-00OR22725. Available at https://info.ornl.gov/sites/publications/Files/Pub57715.pdf. URL: https://info.ornl.gov/sites/publications/Files/Pub57715.pdf.

[6] John F. O'Hanlon. *A User's Guide to Vacuum Technology*. John Wiley & Sons, Hoboken, NJ, 3 edition, 2003.

[7] Leo Brewer, Paul W. Gilles, and Francis A. Jenkins. The vapor pressure and heat of sublimation of graphite. *The Journal of Chemical Physics*, 16(8):797–807, 1948. doi:10.1063/1.1746999.

[8] L. S. Darken and R. W. Gurry. *Physical Chemistry of Metals*. Metallurgy and Metallurgical Engineering Series. McGraw-Hill, New York, NY, USA, 1953. OCLC 544719. Catalog record: https://search.worldcat.org/oclc/544719. URL: https://search.worldcat.org/oclc/544719.

References

[9] Union Carbide Corporation, Carbon Products Division. *The Industrial Graphite Engineering Handbook*. Union Carbide Corporation, New York, NY, USA, 1969. Vapor-pressure data tables reproduced in Ref. [5]. Scanned copy: https://nucleus.iaea.org/sites/graphiteknowledgebase/Meetings2/Old%20Meetings/2017/Background%20Info/GraphiteHandbook.pdf. URL: https://nucleus.iaea.org/sites/graphiteknowledgebase/Meetings2/Old%20Meetings/2017/Background%20Info/GraphiteHandbook.pdf.

[10] F. Abusaif et al. *Storage ring to search for electric dipole moments of charged particles: Feasibility study*, volume 3 of *CERN Yellow Reports: Monographs*. CERN, Geneva, June 2021. arXiv:1912.07881, doi:10.23731/CYRM-2021-003.

[11] Alfons Khoukaz. Internal targets for the PANDA experiment. In *Proceedings of the 8th International Conference on Nuclear Physics at Storage Rings (STORI11)*, volume STORI11 of *Proceedings of Science*, page 036, 2011. doi:10.22323/1.150.0036.

[12] Andrzej Pyszniak et al. A pellet tracking system for hadron physics experiments. In *EPJ Web of Conferences*, volume 66, page 11031, 2014. doi:10.1051/epjconf/20146611031.

[13] William R. Leo. *Techniques for Nuclear and Particle Physics Experiments: A How-to Approach*. Springer, Berlin, 2 edition, 1994.

Backup material

Backup: Carbon film material parameters

geometry

Property	Unit	a-C	sputt./evap.	graphitic/CVD
Thermal conductivity κ	$\mathrm{W\,m^{-1}K^{-1}}$	0.1–1.0	0.3–1.5	2–10
Density ρ	$\mathrm{kg\,m^{-3}}$	2000	2200 / 1900	1700
Specific heat c_p	$\mathrm{J\,kg^{-1}K^{-1}}$	700–900	700–900	700–800
Emissivity ε	–	0.75–0.95	0.8–0.95	0.8–0.95
Strip resistance R_{strip}	MΩ	–	200–800 unexposed, ∼1 after beam	
Residual film stress σ_{res}	MPa	10^2–10^3	10^2–10^3	process dependent

Talk baseline (graphitic/CVD):

- $\kappa = 5\,\mathrm{W\,m^{-1}\,K^{-1}}$, $\rho = 1700\,\mathrm{kg\,m^{-3}}$, $c_p = 750\,\mathrm{J\,kg^{-1}\,K^{-1}}$, $\varepsilon = 0.85$.

Thin-film properties, not bulk graphite: κ sits 1–2 orders below bulk ($390\,\mathrm{W\,m^{-1}\,K^{-1}}$).

Backup: Video-derived observational quantities

observations

Quantity	Effective value	Use in model
Visible strip length scale	$\ell_{\mathrm{vis}} \simeq 25\,\mathrm{mm}$	video-to-mm calibration
Beam-visible interval	$\Delta t_{\mathrm{beam}} \sim 1.5\,\mathrm{s}$	scan timing near beam
Scan speed near beam	$v_t \sim 4\,\mathrm{mm\,s^{-1}}$	moving-source estimates
Projected strip displacement	$\Delta x_{\mathrm{proj}} \sim 3\,\mathrm{mm}$	force-scale estimate
Visible end-glow length	6 to 12 mm	RF end-heating scale

Projected, camera-plane quantities; out-of-plane motion was not measured, so displacements are lower bounds.

These scales anchor the thermal, force, and RF estimates that follow.

Backup: Beam-parameter input cases (full)

◂ beam cases

Quantity	Unit	RHIC flattop	EIC inj. before cool.	EIC inj. after cool.	EIC flattop large ε	EIC flattop cooled ε
Location	–	IP12 pC	IP4	IP4	IP4	IP4
$E_{\mathbf{beam}}$	GeV	250	23.5	23.5	275	275
N_p	10^{10}	20	27.6	27.6	6.9	6.9
$Q_b = N_p Ze$	nC	32.0	44.2	44.2	11.1	11.1
N_b	–	120	290	290	1160	1160
σ_L	m	0.55	0.24	0.24	0.06	0.06
$\sigma_t = \sigma_L/(\beta c)$	ns	1.83	0.80	0.80	0.20	0.20
$I_b^{\mathbf{pk}} = Q_b/(\sqrt{2\pi}\,\sigma_t)$	A	6.97	22.0	22.0	22.0	22.0
$f_{\mathbf{rev}}$	kHz	78.19	78.13	78.13	78.19	78.19
$\tau_b = \tau_{\mathbf{rev}}/N_b$	ns	106.6	44.1	44.1	11.0	11.0
$f_b = 1/\tau_b$	MHz	9.38	22.7	22.7	90.7	90.7
$I_{\mathbf{avg}} = N_b N_p Zef_{\mathbf{rev}}$	A	0.301	1.002	1.002	1.003	1.003
ε_x^n	µm	2.5	3.3	3.3	3.3	3.3
ε_y^n	µm	2.5	3.3	0.3	3.3	0.3
β_x	m	25.41	93.6	93.6	230.3	230.3
β_y	m	28.43	39.59	39.59	69.9	69.9
σ_x	mm	0.488	3.513	3.513	1.610	1.610
σ_y	mm	0.516	2.285	0.689	0.887	0.267
$\sigma_x^{\mathbf{95}} = \sqrt{5.991}\,\sigma_x$	mm	1.195	8.600	8.600	3.942	3.942
$\sigma_y^{\mathbf{95}} = \sqrt{5.991}\,\sigma_y$	mm	1.264	5.593	1.686	2.172	0.655
$\Phi_{\mathbf{0}} = I_{\mathbf{avg}}/(Ze\,2\pi\sigma_x\sigma_y)$	$10^{\mathbf{23}}$ m$^{-\mathbf{2}}$ s$^{-\mathbf{1}}$	11.84	1.240	4.113	6.973	23.13

Backup: Injection flux maps

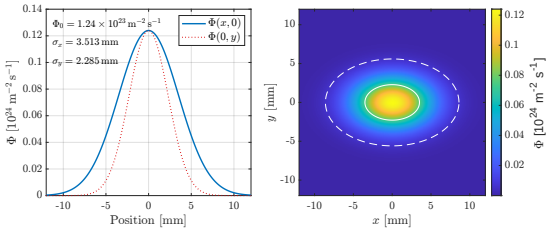

EIC injection, before cooling

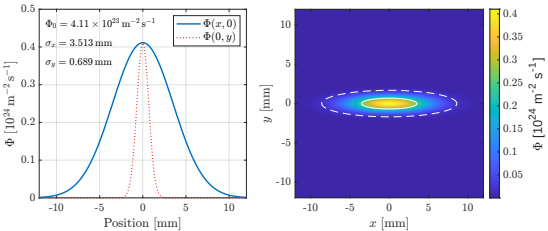

EIC injection, after cooling

– Same injection optics and bunch structure; cooling shrinks σ_y by a factor $\sim$3.3.

Cooling raises Φ_0 already at injection: $1.2 \rightarrow 4.1 \times 10^{23}\,\mathrm{m^{-2}\,s^{-1}}$.

◂ flux maps

Backup: Target-length and scan-direction margins

back

Machine	Beam	Cooling	Orientation	θ [°]	ℓ [mm]	$\sigma_{\parallel}^{95}(\theta)$ [mm]	M_{ℓ}^{95}	$\sigma_{\perp}^{95}(\theta)$ [mm]
RHIC	flattop	—	horizontal	0	25	1.195	10.5	1.264
			vertical	90	25	1.264	9.89	1.195
EIC	injection	no cooling	horizontal	0	50	8.600	2.91	5.593
			diagonal	$\pm$45	50	7.254	3.45	7.254
			vertical	90	50	5.593	4.47	8.600
		cooling	horizontal	0	50	8.600	2.91	1.686
			diagonal	$\pm$45	50	6.197	4.03	6.197
			vertical	90	50	1.686	14.8	8.600
EIC	flattop	no cooling	horizontal	0	50	3.942	6.34	2.172
			diagonal	$\pm$45	50	3.183	7.85	3.183
			vertical	90	50	2.172	11.5	3.942
		cooling	horizontal	0	50	3.942	6.34	0.655
			diagonal	$\pm$45	50	2.826	8.85	2.826
			vertical	90	50	0.655	38.2	3.942

Projected 95 % beam sizes from Eqs. (23) and (24); margin M_{ℓ}^{95} from Eq. (26). Diagonal $\pm 45^{\circ}$ keeps $M_{\ell}^{95} \geq 3.4$ in all EIC cases; steeper angles ($\theta \simeq 70$ to 75°) reach $M_{\ell}^{95} \simeq 9$ to 10 at the price of less symmetric scan directions.

Backup: Roll-averaged chord through the strip

back

- projected width under roll ψ: $W_\perp(\psi) = w\cos\psi + t\sin\psi$
- summing chords over all impact parameters b sweeps the cross section exactly once, $\int \ell_{\mathrm{chord}}\,\mathrm{d}b = wt$, so

$$\langle \ell_{\mathrm{chord}} \rangle_b(\psi) = \frac{wt}{w\cos\psi + t\sin\psi} \qquad (t \text{ face-on, } w \text{ edge-on})$$

- roll average, ψ uniform on $[0, \pi/2]$, evaluates in closed form:

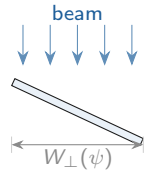

nominal $w/t = 200$ ($w = 10\,\mu\mathrm{m}$, $t = 50\,\mathrm{nm}$):

$\langle \ell_{\mathrm{chord}} \rangle_\psi = 0.191\,\mathrm{m} = 3.817\,t$

$$\langle \ell_{\mathrm{chord}} \rangle_\psi = \frac{2}{\pi}\int_0^{\pi/2} \frac{wt\,\mathrm{d}\psi}{w\cos\psi + t\sin\psi} = \frac{2wt}{\pi\sqrt{w^2+t^2}}\,\ln\frac{\left(\sqrt{w^2+t^2}+w\right)\left(\sqrt{w^2+t^2}+t\right)}{wt}$$

thin strip ($w \gg t$): $\langle \ell_{\mathrm{chord}} \rangle_\psi \simeq (2t/\pi)\ln(2w/t)$, logarithmic in the aspect ratio; sensitivities obey $\eta_w + \eta_t = 1$, and $\Delta w/w = \Delta t/t = 5\,\%$ gives $\Delta\langle\ell\rangle/\langle\ell\rangle = 4.3\,\%$

F. Rathmann, Mean chord length through a rolled rectangular strip, June 2026.

Backup: energy dependence of f_{esc}

$$T_{\max} \simeq 2 m_e c^2 \, \beta^2 \gamma^2, \qquad \frac{dN}{dT} \propto \frac{1}{T^2} \quad (T \leq T_{\max})$$

f_{esc} is the share of the loss carried off by delta electrons that outrange the 50 nm strip: it tracks how hard the knock-on spectrum is relative to the fixed (keV-scale) escape threshold.

Rise ($T_p \lesssim$ 2–3 GeV)

- proton still becoming relativistic, $\beta \to 1$: $T_{\max} \propto \beta^2\gamma^2$ grows, the spectrum hardens, more loss escapes
- the soft, locally absorbed part falls as $1/\beta^2$ (Bethe), so the escaping share keeps climbing

Plateau ($\beta\gamma \gtrsim$ 3–4)

- $\beta \approx 1$ saturates; the restricted (local) stopping power reaches its Fermi plateau and stays flat
- the relativistic rise of the loss goes entirely into escaping deltas, so S_{esc} and $S_{\mathrm{C}}^{\mathrm{SI}}$ rise together and the ratio is fixed

- the knee is the onset of full relativistic motion ($M_p c^2 \simeq 0.94$ GeV), not a material energy; it coincides with the Bethe minimum of ΔE_{loss} (panels c, d), where the rise sits in ΔE_{esc} while ΔE_{heat} stays flat back

Rise: $T_{\max} \propto \beta^2\gamma^2$ still grows; plateau: $\beta = 1$, the added loss all escapes.

Backup: thermal-model input parameters

Quantity	Symbol	Value	Unit
Carbon scenario	–	graphitic/CVD carbon	–
Density	ρ	1700	$\mathrm{kg\,m^{-3}}$
Specific heat capacity	c_p	750	$\mathrm{J\,kg^{-1}\,K^{-1}}$
Thermal conductivity	κ	5	$\mathrm{W\,m^{-1}\,K^{-1}}$
Emissivity	ε	0.85	–
Strip width	w	10	µm
Strip thickness	t	50	nm
Reference RHIC active length	ℓ_{RHIC}	25	mm
Benchmark EIC active length	ℓ_{EIC}	50	mm
Reference target scan speed	v_t	4	$\mathrm{mm\,s^{-1}}$
Holder temperature	T_0	300	K
Effective heat-source scale	η_{heat}	from escape and chord model	

Graphitic/CVD thin-film scenario; the scan speed is the video-derived near-beam scale. η_{heat} converts the nominal flat-layer stopping-power source into the retained heat source (secondary-electron escape and roll-averaged chord).

back

Backup: stopping-power treatment

back

- Standard Bethe–Bloch formalism, evaluated from the projectile charge state, mass, and velocity with the same carbon material assumptions as the rest of the model [13]
- Proton cross-check: the direct evaluation reproduces the tabulated normalization behind the retained-heat scale to within 1–2 %, which accounts for the small offsets in the quoted η_{heat} values
- Tabulated ^{3}He stopping powers are not available over the required energy range (the ASTAR database covers only ^{4}He), so Bethe–Bloch is evaluated directly for the light-ion cases
- One implementation for p and $^{3}\mathrm{He}^{++}$: no separate light-ion normalization, keeping the comparison internally consistent

Backup: dynamic peak temperatures

Machine	Species	Condition	$T_{\max}^{\mathrm{dyn}}$ [K]
Booster	p	injection	611
Booster	p	extraction	662
Booster	^{3}He	injection	724
Booster	^{3}He	extraction	775
AGS	p	injection	401
AGS	p	extraction	710
AGS	^{3}He	injection	454
AGS	^{3}He	extraction	808

Booster/AGS rows: largest width in the scan, $w = 125\,\mu\mathrm{m}$.

Machine/species	Beam condition	Target	$T_{\max}^{\mathrm{dyn}}$ [K]
RHIC p	flattop	vertical	2449
RHIC ^{3}He	flattop reference	horizontal	3111
EIC p	injection before cooling	diagonal	1321
EIC p	injection after cooling	horizontal	1782
EIC p	flattop large emittance	diagonal	2149
EIC p	flattop cooled emittance	diagonal	2900
EIC ^{3}He	injection before cooling	diagonal	1669
EIC ^{3}He	injection after cooling	horizontal	2252
EIC ^{3}He	flattop large emittance	vertical	2731
EIC ^{3}He	flattop cooled emittance	vertical	3685

RHIC/EIC rows: hottest geometry per beam condition; $v_{\mathrm{t}} = 4\,\mathrm{mm\,s^{-1}}$ throughout.

back

Backup: beam removal by nominal and survival-equivalent targets

Case	F_A	σ_{loss} [mb]	Removal/pass	$\Delta_{\mathcal{L}}$ per fill
RHIC p, nominal strip	1	250–300	$(2.1\text{–}2.5)\times10^{-5}$	$(6.3\text{–}7.5)\times10^{-5}$
EIC p flattop, survival-equiv.	2.1×10^{2}	250–300	0.44–0.52 %	1.3–1.6 %
RHIC ^{3}He, survival-equiv.	2.0×10^{3}	1000	15.3 %	38.5 %
EIC ^{3}He flattop, survival-equiv.	1.7×10^{5}	1000	$\simeq$ 100 %	$\simeq$ 100 %

- $F_A = A_{\mathrm{C}}/A_{\mathrm{C},0}$ scales the carbon cross section so the target survives a RHIC-like number of measurements before being consumed
- Single-passage removal exponent $\mu_{\mathrm{pass}} = f_{\mathrm{rev}}\frac{\rho A_{\mathrm{C}}}{v_t}\frac{N_{\mathrm{A}}}{A_{\mathrm{mol}}}\sigma_{\mathrm{loss}} = 8.33\times10^{-8}\,\sigma_{\mathrm{loss}}[\mathrm{mb}]\,F_A$; removal per pass $= 1-\mathrm{e}^{-\mu_{\mathrm{pass}}}$
- Luminosity-weighted loss per fill $\Delta_{\mathcal{L}} = 1-\frac{1}{2}\left(\mathrm{e}^{-2\mu_{\mathrm{pass}}}+\mathrm{e}^{-4\mu_{\mathrm{pass}}}\right)\simeq 3\mu_{\mathrm{pass}}$: three in-and-out measurements per fill, the end-of-fill scan carries no future-luminosity penalty

back

Backup: what changed vs. Thieberger's survival estimate

Thieberger's Excel model

- 1D finite-difference heat equation; static Gaussian beam; radiation from two faces ($\varepsilon = 0.8$) plus neighbour conduction; no target motion
- Bulk-like film: $\kappa = 390\,\mathrm{W/(m\,K)}$, $\rho = 2.26\,\mathrm{g/cm^3}$, $c_p = 0.72\,\mathrm{J/(g\,K)}$, $t = 50\,\mathrm{nm}$; full stopping power retained
- Two source simplifications offset: no secondary-electron escape ($\times 3.3$ high) and nominal-thickness chord ($\times 3.8$ low) nearly cancel: retained source within $\sim 15\%$ of the full model
- Survival test: strip survives if peak T stays below a fixed 2500 K limit; RHIC ($\simeq 2400\,\mathrm{K}$) clears it

What this work changes

- RHIC peak temperatures agree ($\simeq 2400\,\mathrm{K}$ vs. $2449\,\mathrm{K}$): the criterion changed, not the heating
- Fixed limit $\rightarrow$ integrated recession $f_{\mathrm{sub}} = \Delta h_{\mathrm{sub}}/t$ with exponential $v_{\mathrm{sub}}(T)$: loss continues below any limit
- At $\simeq 2400\,\mathrm{K}$ the integrated loss is already percent-per-cycle: finite lifetime, as observed
- Even tightening the cutoff to 2500 K (from the 3650 K reference) still clears RHIC, yet the strip erodes: thresholds ignore the rate

Differences in κ (bulk 390 vs. thin film 5), heat retention, window, and target motion shift per-case temperatures, not the conclusion. P. Thieberger, PolarimeterTargetBeamHeatingSimulation.xlsm

Peak temperatures agree; the integrated-loss criterion changes the verdict.

back